UDC 519.6

# MATHEMATICAL MODELING OF MULTIPHASE MIXTURE INFLOW INTO A STRATIFIED RESERVOIR AND THE BREAKDOWN OF THE LAYERED STRUCTURE

[1] ***Yakhshibaev D.S.,*** [2*] ***Boborakhimov B.I.***

*uzbekpy@gmail.com

[1]Tashkent university of information technologies,
100200, 108, Amir Temur str., Tashkent, Uzbekistan;
[2]Digital technologies and artificial intelligence development research institute,
17A, Buz-2, Tashkent, 100125 Uzbekistan.

A three-dimensional mathematical model is proposed for the inflow of a turbid (sediment-laden) river flow into a density-stratified reservoir, accounting for phase separation and the breakdown of the layered structure. The model is based on Kh.A. Rakhmatulin's theory of interpenetrating continua: the carrier fluid and the dispersed particles each have their own velocity field, and the interphase drag represents particle settling. The vertical mixing coefficient depends on the local Richardson number, capturing stratification breakdown through Kelvin–Helmholtz instability; re-erosion near the bed is modeled by the Garcia–Parker formula. The problem is solved on a Harlow–Welch staggered grid by a five-stage operator-splitting scheme. A simulation of the subcritical plunging regime reproduces the inflow plume, the plunge point, the bottom underflow, and the intrusion layer, and is verified against classical criteria and mass balance.

**Keywords:** stratified reservoir, multiphase flow, Rakhmatulin model, phase separation, turbidity current, plunging, Richardson number, Kelvin–Helmholtz instability, operator splitting, re-erosion, Garcia–Parker formula.

**Citation:** Yakhshibaev D.S., Boborakhimov B.I. 2026. Mathematical modeling of multiphase mixture inflow into a stratified reservoir and the breakdown of the layered structure. *Problems of Computational and Applied Mathematics.* 3(73): 7-24.

**DOI:** https://doi.org/10.71310/pcam.3_73.2026.01

## 1 Introduction

Reservoirs perform vital functions — irrigation, hydropower, water supply and flood protection — yet their useful capacity is shrinking year after year because of sediment accumulation (sedimentation). Recent global assessments have revealed the scale of this process anew: using a physics-informed machine-learning model covering more than 550,000 reservoirs, Woolway et al. showed that the average water volume of reservoirs worldwide is declining by roughly 7.3% per decade, with small reservoirs being the most at risk [1]. Computations by Smakhtin et al. for 47,403 large dams in 150 countries predict the loss of about 26% of global useful capacity by 2050 [2]. To support such assessments with reliable data, open global sediment databases (GRILSS) [3] and methods for estimating sedimentation rates from high-resolution Sentinel-2 satellite imagery and water-level data [4] are being developed. The problem is especially acute for Central Asia: regional rivers such as the Amu Darya, the Syr Darya and the Zarafshan carry high sediment loads, and many reservoirs in Uzbekistan are severely affected by intense sedimentation [5].

When turbid river water enters clear, stratified reservoir water, its density exceeds that of the surroundings, so it "plunges" downward and turns into a dense bottom-hugging current — a turbidity current. The hydrodynamic mechanisms of this phenomenon have been

reviewed in detail by Meiburg and Kneller [6], while the classical foundations of plunging theory lie in the works of Akiyama and Stefan [21] and Ellison and Turner [22]. Using a two-layer depth-averaged model, Sun et al. analyzed the effect of tributary inflow on a reservoir turbidity current, including the shift of the plunge point [7]. Field observations by Blanckaert et al. in a deep stratified lake showed that mixing in the plunge zone and resuspension of sediment from the bed play decisive roles along the path of a dense river inflow [8]. Rétif et al. predicted the intrusion depth and vertical density structure of a gravity current entering a two-layer stratification from laboratory experiments through a critical Froude number [9].

To predict such processes quantitatively, one-dimensional (1D), two-dimensional depth- or layer-averaged (2D), and fully three-dimensional computational fluid dynamics (3D CFD) models are employed. In a comprehensive review, Greimann summarized best practices for modeling reservoir sediment flushing and turbidity-current venting, emphasizing that many empirical models cannot describe sediment transport after deposition and that advanced 2D/3D models are therefore required [10]. Guo et al. provided a comparative survey of the current state of turbidity-current modeling — single-fluid (one-fluid) and two-fluid models, high-resolution methods, and artificial intelligence approaches [11].

The most complete physical description of a sediment–water mixture is the two-fluid (Euler–Euler) approach, which treats both phases as interpenetrating continua; the classical theoretical foundation of this approach was laid by Kh.A. Rakhmatulin [12]. Unlike single-fluid Boussinesq models, the two-fluid model assigns a separate velocity field to each phase (water and particles) and thus directly represents phase separation — the settling of particles relative to the water. Based on an equilibrium closure, Balachandar derived a simplified two-fluid model for a dilute dispersion of small particles and distinguished three regimes according to the relative strength of gravitational settling [13]. Mathieu, Chauchat et al. coupled the water and sediment phases together with a free surface (air phase) in an Eulerian framework in the OpenFOAM-based `sedInterFoam` model to simulate multiphase sediment transport [14].

The incoming flow generates velocity shear near the existing interface, lowering the local Richardson number $Ri$; when $Ri$ drops below a critical value ($Ri < 1/4$), Kelvin–Helmholtz (KH) instability develops, the layers mix, and stratification is destroyed. Olsthoorn et al. studied asymmetric shear instabilities with mismatched velocity and density interfaces, analyzing their hybrid character between the KH and Holmboe regimes and the distribution of the gradient Richardson number [15]. Li and Lin numerically modeled KH instability in a variable-density stratification, showing that the instability enhances mixing through interface growth, while diffusion broadens the transition layer [16]. At the same time, stable stratification reduces the entrainment of ambient water by a turbidity current, allowing it to travel over long distances [17]; the theoretical description of long-runout turbidity currents has recently been developed in a two-layer formulation [18].

The near-bed turbulence of a turbidity current lifts deposited particles, giving rise to re-erosion that competes with settling. In computing the intensity of sediment entrainment from the bed into suspension, the widely used empirical relations of Garcia and Parker serve as the principal criterion [19]. From a practical viewpoint, selective withdrawal is an important tool in managing stratified reservoirs and has demonstrated its effectiveness in stabilizing thermal stratification and improving downstream ecological conditions [20].

A review of the existing literature shows that most works on modeling turbid river inflow into a reservoir rely on 2D depth-/layer-averaged or single-fluid Boussinesq approx-

imations; studies that consider phase separation (particle settling) and the destruction of the existing stratification simultaneously, together with re-erosion at the bed, within a fully three-dimensional two-fluid Rakhmatulin model are rare. To fill precisely this gap, the present work poses — in three-dimensional geometry, on the basis of Kh.A. Rakhmatulin's full two-fluid model — the dynamics of the inflow of a multiphase mixture into a stratified reservoir, phase separation, and the breakdown of the layered structure, and investigates them numerically using an adaptive scheme based on operator splitting.

## 2 Problem statement and mathematical model

We consider a rectangular reservoir with horizontal dimensions $L_x \times L_y$ and depth $H$. In the initial state the reservoir has a two-layer structure: the upper layer is clear water (thickness $h_1 = H - \zeta_0$, particle volume concentration $\varphi_1 \approx 0$), and the lower layer is turbid water (thickness $h_2 = \zeta_0$, concentration $\varphi_2$), with the interface located at $z = \zeta_0$. River flow enters through the surface at $x = 0$. The river water is a two-phase dispersed mixture consisting of a carrier medium (water, $n = 1$) and dispersed particles (sediment, $n = 2$); the inflow concentration satisfies $\varphi_{\text{in}} > \varphi_2 > \varphi_1$, i.e. the river water is more turbid than either layer of the reservoir. The mean velocity $U_{\text{in}}$, depth $h_{\text{in}}$ and width $b_{\text{in}}$ of the river flow are prescribed. The physical scheme of the problem is shown in Figure 1.

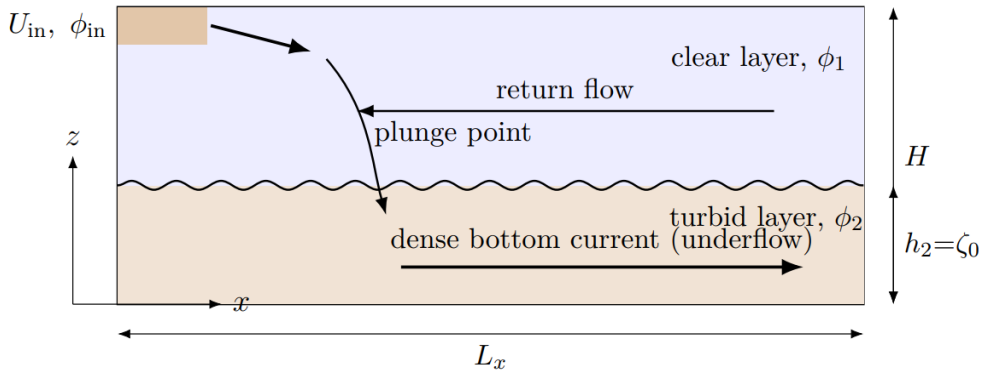


**Figure 1** Physical scheme of multiphase river inflow into a stratified reservoir and of the plunging process (vertical cross-section)

The computational domain and the river inflow surface are

$$\Omega = \{(x, y, z) : 0 \leqslant x \leqslant L_x,\ 0 \leqslant y \leqslant L_y,\ 0 \leqslant z \leqslant H\},$$

$$\Gamma_{\text{in}} = \{x = 0,\ |y - y_{\text{in}}| \leqslant b_{\text{in}}/2,\ 0 \leqslant z \leqslant h_{\text{in}}\}.$$

Each phase has its own velocity field. The unknown functions are: the velocity components of the water phase ($n = 1$) $u_1, v_1, w_1$; the velocity components of the particle phase ($n = 2$) $u_2, v_2, w_2$; the pressure $p$; and the particle volume concentration $\varphi$ — eight unknown functions in total (Table 1).

On the basis of Kh.A. Rakhmatulin's model of interpenetrating multiphase media [12], the Reynolds-averaged equations are written as follows.

*Continuity equation for the particle phase:*

$$\begin{gathered}\frac{\partial \varphi}{\partial t}+\frac{\partial(\varphi u_2)}{\partial x}+\frac{\partial(\varphi v_2)}{\partial y}+\frac{\partial(\varphi w_2)}{\partial z}= \\ =\frac{\partial}{\partial x}\left(D_h \frac{\partial \varphi}{\partial x}\right)+\frac{\partial}{\partial y}\left(D_h \frac{\partial \varphi}{\partial y}\right)+\frac{\partial}{\partial z}\left(D_z \frac{\partial \varphi}{\partial z}\right).\end{gathered} \tag{1}$$

*Continuity equation for the water phase:*

$$\begin{gathered}-\frac{\partial \varphi}{\partial t}+\frac{\partial\left[(1-\varphi) u_1\right]}{\partial x}+\frac{\partial\left[(1-\varphi) v_1\right]}{\partial y}+\frac{\partial\left[(1-\varphi) w_1\right]}{\partial z}= \\ =-\frac{\partial}{\partial x}\left(D_h \frac{\partial \varphi}{\partial x}\right)-\frac{\partial}{\partial y}\left(D_h \frac{\partial \varphi}{\partial y}\right)-\frac{\partial}{\partial z}\left(D_z \frac{\partial \varphi}{\partial z}\right).\end{gathered} \tag{2}$$

Adding these two equations yields the incompressibility condition of the mixture:

$$\frac{\partial V_x}{\partial x}+\frac{\partial V_y}{\partial y}+\frac{\partial V_z}{\partial z}=0, \quad \begin{aligned} V_x &= (1-\varphi) u_1+\varphi u_2, \\ V_y &= (1-\varphi) v_1+\varphi v_2, \\ V_z &= (1-\varphi) w_1+\varphi w_2, \end{aligned} \tag{3}$$

where $V_x, V_y, V_z$ are the mean volumetric velocity components.

Momentum equations for the particle phase (the $x, y, z$ projections):

$$\begin{gathered}\varphi \rho_s\left(\frac{\partial u_2}{\partial t}+u_2 \frac{\partial u_2}{\partial x}+v_2 \frac{\partial u_2}{\partial y}+w_2 \frac{\partial u_2}{\partial z}\right)= \\ =-\varphi \frac{\partial p}{\partial x}+\varphi \mu_{\text{eff}}\left(\frac{\partial^2 u_2}{\partial x^2}+\frac{\partial^2 u_2}{\partial y^2}+\frac{\partial^2 u_2}{\partial z^2}\right)+\beta(\varphi)(u_1-u_2),\end{gathered} \tag{4}$$

$$\begin{gathered}\varphi \rho_s\left(\frac{\partial w_2}{\partial t}+u_2 \frac{\partial w_2}{\partial x}+v_2 \frac{\partial w_2}{\partial y}+w_2 \frac{\partial w_2}{\partial z}\right)= \\ =-\varphi \frac{\partial p}{\partial z}+\varphi \mu_{\text{eff}}\left(\frac{\partial^2 w_2}{\partial x^2}+\frac{\partial^2 w_2}{\partial y^2}+\frac{\partial^2 w_2}{\partial z^2}\right)-\varphi \rho_s g+\beta(\varphi)(w_1-w_2).\end{gathered} \tag{5}$$

**Table 1** Main variables and parameters of the model

| Symbol | Meaning | Unit |
|---|---|---|
| $u_1, v_1, w_1$ | velocity components of the water phase | m/s |
| $u_2, v_2, w_2$ | velocity components of the particle phase | m/s |
| $V_x, V_y, V_z$ | mean volumetric velocity components | m/s |
| $p$ | pressure | Pa |
| $\varphi$ | particle volume concentration | — |
| $\rho_f, \rho_s$ | density of water and of a particle | $\mathrm{kg/m^3}$ |
| $\rho_0$ | reference (characteristic) density | $\mathrm{kg/m^3}$ |
| $\mu_f$ | dynamic viscosity of water | $\mathrm{Pa \cdot s}$ |
| $\mu_{\text{eff}}$ | effective (turbulent) viscosity | $\mathrm{Pa \cdot s}$ |
| $d$ | particle diameter | m |
| $w_{\text{St}}$ | Stokes settling velocity of a single particle | m/s |
| $w_s(\varphi)$ | hindered settling velocity | m/s |
| $n_R$ | hindered-settling exponent | — |
| $D_h, D_z$ | horizontal and vertical diffusion coefficient | $\mathrm{m^2/s}$ |
| $\beta(\varphi)$ | interphase drag coefficient | $\mathrm{kg/(m^3 \cdot s)}$ |
| $g$ | gravitational acceleration | $\mathrm{m/s^2}$ |
| $g'$ | reduced gravitational acceleration | $\mathrm{m/s^2}$ |
| Ri | Richardson number | — |
| $E_r$ | re-erosion intensity | m/s |
| $C_f$ | bed friction coefficient | — |
| $\mathrm{Re}_p$ | particle Reynolds number | — |
| $\delta_i, \zeta_0$ | interface thickness and level | m |

Momentum equations for the water phase (the $x, y, z$ projections):

$$\begin{aligned}(1-\varphi)\rho_f\left(\frac{\partial u_1}{\partial t}+u_1\frac{\partial u_1}{\partial x}+v_1\frac{\partial u_1}{\partial y}+w_1\frac{\partial u_1}{\partial z}\right)=\\ =-(1-\varphi)\frac{\partial p}{\partial x}+(1-\varphi)\mu_{\text{eff}}\left(\frac{\partial^2 u_1}{\partial x^2}+\frac{\partial^2 u_1}{\partial y^2}+\frac{\partial^2 u_1}{\partial z^2}\right)-\beta(\varphi)(u_1-u_2),\end{aligned} \tag{6}$$

$$\begin{aligned}(1-\varphi)\rho_f\left(\frac{\partial v_1}{\partial t}+u_1\frac{\partial v_1}{\partial x}+v_1\frac{\partial v_1}{\partial y}+w_1\frac{\partial v_1}{\partial z}\right)=\\ =-(1-\varphi)\frac{\partial p}{\partial y}+(1-\varphi)\mu_{\text{eff}}\left(\frac{\partial^2 v_1}{\partial x^2}+\frac{\partial^2 v_1}{\partial y^2}+\frac{\partial^2 v_1}{\partial z^2}\right)-\beta(\varphi)(v_1-v_2),\end{aligned} \tag{7}$$

$$\begin{aligned}(1-\varphi)\rho_f\left(\frac{\partial w_1}{\partial t}+u_1\frac{\partial w_1}{\partial x}+v_1\frac{\partial w_1}{\partial y}+w_1\frac{\partial w_1}{\partial z}\right)=\\ =-(1-\varphi)\frac{\partial p}{\partial z}+(1-\varphi)\mu_{\text{eff}}\left(\frac{\partial^2 w_1}{\partial x^2}+\frac{\partial^2 w_1}{\partial y^2}+\frac{\partial^2 w_1}{\partial z^2}\right)-(1-\varphi)\rho_f g-\beta(\varphi)(w_1-w_2).\end{aligned} \tag{8}$$

By Newton's third law, the interphase forces are antisymmetric: the force on the particles is $+\beta(\varphi)(\cdot)$, and on the water $-\beta(\varphi)(\cdot)$. It is precisely these terms that equilibrate the two phase velocities and establish a steady settling velocity.

Interphase drag coefficient and steady settling velocity:

$$\beta(\varphi) = \frac{18\mu_f\varphi}{d^2}(1-\varphi)^{1-n_R}, \quad w_s(\varphi) = w_{\mathrm{St}}(1-\varphi)^{n_R}, \tag{9}$$

where $d$ is the particle diameter, $w_{\mathrm{St}}$ is the Stokes settling velocity of a single particle, and $n_R$ is the hindered-settling exponent. As the concentration increases ($\varphi \to 1$), settling slows down — the hindered-settling effect.

The vertical diffusion coefficient is taken as a function of the strength of the stratification:

$$D_z = \frac{D_{z0}}{(1+\sigma_R \mathrm{Ri})^{n_d}}, \quad \mathrm{Ri}(x,y,z,t) = \frac{g(\rho_s-\rho_f)/\rho_0}{\left(\dfrac{\partial V_x}{\partial z}\right)^2 + \left(\dfrac{\partial V_y}{\partial z}\right)^2 + \varepsilon_{\mathrm{Ri}}} \left|\frac{\partial \varphi}{\partial z}\right|. \tag{10}$$

This relation embodies two competing mechanisms: when particles settle ($\partial\varphi/\partial z < 0$), the stratification strengthens, $Ri$ increases, $D_z$ decreases and mixing weakens (a stabilizing effect); when the river flow enters, the velocity shear grows, $Ri$ decreases, $D_z$ increases and mixing intensifies (a destabilizing effect).

At $t = 0$ the reservoir is at rest and a two-layer stratification is present:

$$u_1 = v_1 = w_1 = 0, \quad u_2 = v_2 = w_2 = 0, \tag{11}$$

$$\varphi(x,y,z,0) = \frac{\varphi_2}{2}\left[1 - \tanh\left(\frac{z-\zeta_0}{\delta_i}\right)\right], \tag{12}$$

$$p(x,y,z,0) = p_{\mathrm{atm}} + \int_z^H [\rho_f(1-\varphi) + \rho_s\varphi]\, g\, d\xi, \tag{13}$$

where $\delta_i$ is the initial interface thickness and the pressure follows the hydrostatic distribution.

**River inflow surface** ($\Gamma_{\mathrm{in}}$). The phases are assumed to be in equilibrium in the river flow:

$$u_1 = u_2 = U_{\mathrm{in}}, \quad v_1 = v_2 = 0, \quad w_1 = w_2 = 0, \quad \varphi = \varphi_{\mathrm{in}}, \qquad (y,z) \in \Gamma_{\mathrm{in}}. \tag{14}$$

Outside the inflow region, no-slip / no-flux (solid-wall) conditions are imposed on the surface $x = 0$, on the opposite wall $x = L_x$, and on the side walls $y = 0$, $y = L_y$.

**Bed surface** ($z = 0$). No-slip is imposed for the water phase; for the particle phase the horizontal velocities vanish and the vertical velocity equals the settling velocity:

$$u_1 = v_1 = w_1 = 0, \qquad u_2 = v_2 = 0, \qquad w_2 = -w_s(\varphi)\big|_{z=0}. \tag{15}$$

For the concentration, the balance of settling and re-erosion holds:

$$\left(-\varphi w_s(\varphi) + D_z\frac{\partial\varphi}{\partial z}\right)\Big|_{z=0} = E_r(x,y,t). \tag{16}$$

The re-erosion intensity is computed as a function of the near-bed flow velocity using the Garcia–Parker formula:

$$E_r = \frac{A_r Z_r^5}{1 + A_r Z_r^5/0.3} w_s(\varphi)\Big|_{z=0}, \quad Z_r = \frac{u_* \mathrm{Re}_p^{0.6}}{w_{\mathrm{St}}}, \quad u_* = \sqrt{C_f(u_1^2+v_1^2)|_{z=\Delta z/2}}, \tag{17}$$

where $\mathrm{Re}_p = \rho_f w_{\mathrm{St}} d/\mu_f$ is the particle Reynolds number, $A_r = 1{,}3 \times 10^{-7}$, and $C_f$ is the friction coefficient.

**Free surface** ($z = H$). The tangential stresses vanish for the water and particle phases, the normal velocity is zero, the pressure equals the atmospheric pressure, and no particles leave through the surface:

$$\frac{\partial u_n}{\partial z} = \frac{\partial v_n}{\partial z} = 0, \quad w_n = 0 \ (n = 1, 2), \quad p = p_{\mathrm{atm}}, \quad \left(-\varphi w_s(\varphi) + D_z \frac{\partial \varphi}{\partial z}\right)\Big|_{z=H} = 0. \tag{18}$$

To assess the stability of the stratified flow, the reduced gravitational acceleration and the critical turbidity-current velocity are introduced:

$$g' = g\,\frac{\rho_2 - \rho_1}{\rho_0}, \qquad U_{\mathrm{cr}} = 2\sqrt{\frac{g'(\zeta_0 - h_t/2)^2}{\delta_i}}, \qquad Q_{\mathrm{in,cr}} = 2\,b_{\mathrm{in}}\,h_t\sqrt{\frac{g'(\zeta_0 - h_t/2)^2}{\delta_i}}. \tag{19}$$

The minimum surface area required for clarification and the modified clarification time under the influence of the river inflow are

$$S_{\min} = \frac{Q_{\mathrm{in}}\varphi_{\mathrm{in}}}{w_{\mathrm{St}}(1-\varphi_2)^{n_R}\varphi_2}, \quad T_{\mathrm{cl}}^{(\mathrm{mod})} = \frac{T_{\mathrm{cl}}}{1-\mathcal{R}}, \quad \mathcal{R} = \frac{Q_{\mathrm{in}}\varphi_{\mathrm{in}}}{w_s(\varphi_2)\varphi_2 L_x L_y}. \tag{20}$$

For the stratification to be preserved and clarification to continue, the following three conditions must hold simultaneously:

$$\mathrm{Ri}_\zeta > \frac{1}{4}\ \text{(Kelvin–Helmholtz)}, \quad \frac{U_t^2}{g'\delta_i} < 1\ \text{(internal waves)}, \quad \mathcal{R} < 1\ \text{(mass balance)}. \tag{21}$$

Thus, the governing equations (3)–(13), together with the initial conditions (14)–(16) and the boundary conditions (17)–(21), form the complete, closed three-dimensional statement of the problem: eight unknowns, eight equations, with conditions for all unknowns on all six surfaces.

## 3 Numerical solution algorithm

The computational domain $\Omega$ is covered by a structured rectangular grid: $N_x$ and $N_y$ cells in the horizontal directions and $N_z$ cells in the vertical direction, with corresponding steps $\Delta x = L_x/N_x$, $\Delta y = L_y/N_y$, $\Delta z = H/N_z$. A Harlow–Welch staggered (MAC) grid is used: the scalar quantities — the concentration $\varphi$ and the pressure $p$ — are placed at cell centers $(x_i, y_j, z_k)$, while the velocity components are placed at cell faces. This arrangement eliminates unphysical oscillations in the pressure–velocity coupling.

At the beginning of every step the time step is computed adaptively from the advective Courant–Friedrichs–Lewy (CFL) condition (the diffusive restriction is removed because the Crank–Nicolson scheme is used for the diffusive terms):

$$\Delta t = \frac{Co_{\max}}{\max\limits_{i,j,k}\left(\dfrac{U_d}{\Delta x}, \dfrac{|u|}{\Delta x} + \dfrac{|v|}{\Delta y} + \dfrac{|w|}{\Delta z}\right)}, \qquad Co_{\max} = 0.5, \tag{22}$$

where $U_d = U_{\mathrm{in}}$ is the river inflow velocity.

On the staggered grid the scalar quantities are placed at cell centers $(x_i, y_j, z_k)$, where $x_i = (i - \frac{1}{2})\Delta x$, $y_j = (j - \frac{1}{2})\Delta y$, $z_k = (k - \frac{1}{2})\Delta z$; the $x$-velocity $u$ is defined at the $(i + \frac{1}{2}, j, k)$ faces, $v$ at $(i, j + \frac{1}{2}, k)$, and $w$ at $(i, j, k + \frac{1}{2})$. To compute the concentration fluxes to second order but without unphysical oscillations, the cell-face values are obtained by a total-variation-diminishing (TVD) reconstruction. When the face velocity is positive $(u^n_{i+1/2,j,k} > 0)$:

$$\alpha^{\mathrm{f}}_{i+1/2} = \alpha^n_i + \tfrac{1}{2}\,\psi(r^+_i)\,(\alpha^n_{i+1} - \alpha^n_i), \qquad r^+_i = \frac{\alpha^n_i - \alpha^n_{i-1}}{\alpha^n_{i+1} - \alpha^n_i}, \tag{23}$$

and when it is negative $(u^n_{i+1/2,j,k} < 0)$:

$$\alpha^{\mathrm{f}}_{i+1/2} = \alpha^n_{i+1} - \tfrac{1}{2}\,\psi(r^-_{i+1})\,(\alpha^n_{i+1} - \alpha^n_i), \qquad r^-_{i+1} = \frac{\alpha^n_{i+2} - \alpha^n_{i+1}}{\alpha^n_{i+1} - \alpha^n_i},$$

where the van-Leer-type flux limiter

$$\psi(r) = \frac{r + |r|}{1 + |r|},$$

is adopted; an analogous reconstruction is carried out in the $y$ and $z$ directions and for the velocity components of both phases. The diffusion coefficients at the cell faces are computed as harmonic means:

$$D_{i+1/2,j,k} = \frac{2\,D_{i,j,k}\,D_{i+1,j,k}}{D_{i,j,k} + D_{i+1,j,k}}. \tag{24}$$

Each time step $t^n \to t^{n+1}$ is carried out in five stages.

**Stage 1 (advective predictor step).** The concentration and the velocity fields of both phases are updated under the action of the advective terms alone. For the concentration, the full discrete form with TVD fluxes is

$$\frac{\alpha^*_{i,j,k} - \alpha^n_{i,j,k}}{\Delta t} = -\frac{\alpha^{\mathrm{f}}_{i+1/2}V^n_{x,i+1/2} - \alpha^{\mathrm{f}}_{i-1/2}V^n_{x,i-1/2}}{\Delta x} - \frac{\alpha^{\mathrm{f}}_{j+1/2}V^n_{y,j+1/2} - \alpha^{\mathrm{f}}_{j-1/2}V^n_{y,j-1/2}}{\Delta y} - \frac{\alpha^{\mathrm{f}}_{k+1/2}V^n_{z,k+1/2} - \alpha^{\mathrm{f}}_{k-1/2}V^n_{z,k-1/2}}{\Delta z}.$$

The advective terms of the $x$-momentum equation of the particle phase are discretized with an upwind scheme:

$$\frac{u^*_{2,i,j,k} - u^n_{2,i,j,k}}{\Delta t} = -\begin{cases} u^n_{2,i,j,k}\dfrac{u^n_{2,i,j,k} - u^n_{2,i-1,j,k}}{\Delta x}, & u^n_{2,i,j,k} > 0, \\ u^n_{2,i,j,k}\dfrac{u^n_{2,i+1,j,k} - u^n_{2,i,j,k}}{\Delta x}, & u^n_{2,i,j,k} < 0, \end{cases} - \big[\,y\text{- and } z\text{-direction advective terms (analogous)}\,\big].$$

The remaining components $(v_2, w_2)$ and the momentum equations of the water phase $(u_1, v_1, w_1)$ are discretized in exactly the same manner.

**Stage 2 (diffusive step).** The diffusive terms are approximated to second order in time with the implicit Crank–Nicolson scheme:

$$\frac{\alpha^{**}_{i,j,k} - \alpha^*_{i,j,k}}{\Delta t} = \tfrac{1}{2}\big(\mathcal{L}_x + \mathcal{L}_y + \mathcal{L}_z\big)\alpha^* + \tfrac{1}{2}\big(\mathcal{L}_x + \mathcal{L}_y + \mathcal{L}_z\big)\alpha^{**},$$

where, for example, the discrete form of the $x$-direction diffusion operator is

$$\mathcal{L}_x\alpha = \frac{D_{i+1/2}(\alpha_{i+1}-\alpha_i) - D_{i-1/2}(\alpha_i-\alpha_{i-1})}{\Delta x^2}.$$

The resulting three-dimensional implicit system is solved by the alternating-direction implicit (ADI) method in three successive sweeps; at each sweep a tridiagonal system is formed along a single coordinate and solved by the Thomas algorithm in $O(N)$ operations:

$$\Big(I - \tfrac{\Delta t}{2}\mathcal{L}_x\Big)\widetilde{\alpha} = \Big(I + \tfrac{\Delta t}{2}\mathcal{L}_y + \tfrac{\Delta t}{2}\mathcal{L}_z\Big)\alpha^*,$$

$$\Big(I - \tfrac{\Delta t}{2}\mathcal{L}_y\Big)\widehat{\alpha} = \widetilde{\alpha} - \tfrac{\Delta t}{2}\mathcal{L}_y\alpha^*, \qquad \Big(I - \tfrac{\Delta t}{2}\mathcal{L}_z\Big)\alpha^{**} = \widehat{\alpha} - \tfrac{\Delta t}{2}\mathcal{L}_z\alpha^*.$$

The viscous diffusion of the velocity components of both phases is treated by exactly the same scheme.

**Stage 3 (interphase drag and gravity).** At each node the interphase-drag and gravity terms are accounted for with a semi-implicit scheme — this removes the stiff restriction that arises when the interphase-drag coefficient $\beta(\varphi)$ is large. For the $z$-direction:

$$\rho_s\alpha^{**}\,\frac{w_2^{***}-w_2^{**}}{\Delta t} = K\big(w_1^{***}-w_2^{***}\big) - \rho_s\alpha^{**}g,$$
$$\rho_f(1-\alpha^{**})\,\frac{w_1^{***}-w_1^{**}}{\Delta t} = -K\big(w_1^{***}-w_2^{***}\big) - \rho_f(1-\alpha^{**})g,$$

where $K=\beta(\varphi^{**})$. With the notation $A=\rho_s\alpha^{**}/\Delta t$ and $B=\rho_f(1-\alpha^{**})/\Delta t$, these two equations reduce to a $2\times 2$ linear system:

$$\begin{pmatrix} A+K & -K \\ -K & B+K \end{pmatrix}\begin{pmatrix} w_2^{***} \\ w_1^{***} \end{pmatrix} = \begin{pmatrix} A\,w_2^{**} - \rho_s\alpha^{**}g \\ B\,w_1^{**} - \rho_f(1-\alpha^{**})g \end{pmatrix}.$$

Since its determinant $\Delta = (A+K)(B+K)-K^2 = AB+K(A+B) > 0$, the solution is found analytically in closed form at every node; for the horizontal components the same system without the gravity term is solved.

**Stage 4 (pressure correction, projection).** The intermediate velocity field $\mathbf{V}^{***}$ does not in general satisfy the incompressibility condition; to correct it a pressure correction $p'$ is introduced. The divergence of the mean volumetric velocity is computed to second order at the cell center:

$$(\nabla\cdot\mathbf{V}^{***})_{i,j,k} = \frac{V^{***}_{x,i+1/2}-V^{***}_{x,i-1/2}}{\Delta x} + \frac{V^{***}_{y,j+1/2}-V^{***}_{y,j-1/2}}{\Delta y} + \frac{V^{***}_{z,k+1/2}-V^{***}_{z,k-1/2}}{\Delta z}.$$

A seven-point discrete Poisson equation for the pressure correction is obtained:

$$\frac{p'_{i+1,j,k}-2p'_{i,j,k}+p'_{i-1,j,k}}{\Delta x^2} + \frac{p'_{i,j+1,k}-2p'_{i,j,k}+p'_{i,j-1,k}}{\Delta y^2} +$$
$$+\frac{p'_{i,j,k+1}-2p'_{i,j,k}+p'_{i,j,k-1}}{\Delta z^2} = \frac{\overline{\rho}}{\Delta t}\,(\nabla\cdot\mathbf{V}^{***})_{i,j,k},$$

which is solved by the preconditioned conjugate-gradient (PCG) method; the normal derivative of $p'$ is zero on the inflow surface ($\partial p'/\partial n = 0$) and $p'=0$ on the free surface.

The velocity components are then corrected (through a single pressure field for both phases):

$$u^{n+1}_{n,i+1/2} = u^{***}_{n,i+1/2} - \frac{\Delta t}{\overline{\rho}}\,\frac{p'_{i+1,j,k} - p'_{i,j,k}}{\Delta x},$$

$$w^{n+1}_{n,k+1/2} = w^{***}_{n,k+1/2} - \frac{\Delta t}{\overline{\rho}}\,\frac{p'_{i,j,k+1} - p'_{i,j,k}}{\Delta z}, \qquad n = 1, 2,$$

and the $v$ components are corrected analogously.

**Stage 5 (re-erosion source).** In the cell layer nearest the bed ($k = 1$) the resuspension of deposited particles is taken into account. First the near-bed shear velocity and the Garcia–Parker parameters are computed discretely:

$$u_{*,i,j} = \sqrt{C_f\left(u^2_{1,i,j,1} + v^2_{1,i,j,1}\right)}, \quad Z_{r,i,j} = \frac{u_{*,i,j}\mathrm{Re}_p^{0.6}}{w_{\mathrm{St}}},$$

$$E_{r,i,j} = \frac{A_r Z^5_{r,i,j}}{1 + A_r Z^5_{r,i,j}/0{,}3}\, w_s(\alpha^{**}_{i,j,1}),$$

and then the concentration is updated by the source term (with the physical bound $E_r\Delta t/\Delta z \leqslant \alpha_{\max}$):

$$\alpha^{n+1}_{i,j,1} = \alpha^{**}_{i,j,1} + \frac{\Delta t}{\Delta z}\,E_{r,i,j}.$$

The boundary conditions are implemented by the ghost- (virtual-)cell method. *On the river inflow surface* the face velocities are prescribed directly: $u_{1,1/2,j,k} = u_{2,1/2,j,k} = U_d$, $v = w = 0$; the face value of the concentration is $\alpha^{\mathrm{f}}_{1/2,j,k} = \alpha_{\mathrm{in}}$, and the ghost cell is obtained by extrapolation, $\alpha_{0,j,k} = 2\alpha_{\mathrm{in}} - \alpha_{1,j,k}$. *On the bed surface* (the ghost layer $k = 0$ below $k = 1$) the no-slip condition for water is ensured by $u_{1,i,j,0} = -u_{1,i,j,1}$, while for the particles the concentration gradient is determined from the balance of settling and re-erosion:

$$D_z\frac{\alpha_{i,j,1} - \alpha_{i,j,0}}{\Delta z} = \alpha_{i,j,1}\,w_s(\alpha_{i,j,1}) - E_{r,i,j} \;\Rightarrow\; \alpha_{i,j,0} = \alpha_{i,j,1} - \frac{\Delta z}{D_z}\big[\alpha_{i,j,1}\,w_s - E_{r,i,j}\big].$$

*On the free surface* (the ghost layer above $k = N_z$) a zero-gradient condition is imposed for the velocities and a zero-flux condition for the particles in the form $\alpha_{i,j,N_z+1} = \alpha_{i,j,N_z} - (\Delta z\,w_s/D_z)\,\alpha_{i,j,N_z}$; *on the side walls*, zero-gradient (no-flux) conditions hold for all quantities.

Each time step is carried out in the following sequence:

- the initial values and conditions are set;
- the adaptive $\Delta t$ is computed from (24);
- the river inflow boundary conditions and the near-bed coefficients $u_*$, $E_r$ are updated;
- Stage 1: advective predictor step (TVD);
- Stage 2: diffusive step (Crank–Nicolson + ADI/Thomas);
- Stage 3: interphase drag and gravity (semi-implicit, analytic solution);
- Stage 4: pressure correction — Poisson equation (PCG);
- boundary conditions are imposed on the velocity field and all unknowns;
- Stage 5: re-erosion source;
- Picard iteration for the nonlinear terms: the iteration stops when the relative difference of the velocity field between two successive iterations is smaller than $10^{-8}$;

– convergence is checked and the next step is taken.

## 4 Numerical results and discussion

To demonstrate the capabilities of the scheme, the subcritical plunging regime was modeled in a laboratory-scale prismatic basin. The computational parameters are given in Table 2.

**Table 2** Baseline computational parameters

| Parameter | Symbol | Value |
|---|---|---|
| Domain length | $L_x$ | 4.0 m |
| Domain width | $L_y$ | 2.0 m |
| Domain depth | $H$ | 1.5 m |
| Number of grid cells | $N_x, N_y, N_z$ | 24, 16, 20 |
| Horizontal steps | $\Delta x, \Delta y$ | 0.167; 0.125 m |
| Vertical step | $\Delta z$ | 0.075 m |
| Interface level | $h_i$ | 0.7 m |
| Upper-layer concentration | $\alpha_1$ | $1 \times 10^{-3}$ |
| Lower-layer concentration | $\alpha_2$ | $5 \times 10^{-2}$ |
| Inflow mean velocity | $U_{\text{in}}$ | 0.5 m/s |
| Inflow concentration | $\alpha_{\text{in}}$ | 0.10 |
| Inflow height / width | $h_{\text{in}}, B_{\text{in}}$ | 0.3; 0.6 m |
| Reduced gravity | $g'$ | 0.763 m/s$^2$ |
| Horizontal/vertical diffusion | $D_h, D_v$ | $1 \times 10^{-2}$ m$^2$/s |
| Effective viscosity | $\nu_{\text{eff}}$ | $1 \times 10^{-4}$ m$^2$/s |
| Simulation duration | $t_{\text{end}}$ | 30 s |

The value $g' \approx 0{,}763$ m/s$^2$, corresponding to the density difference, equals about 7.8% of the gravitational acceleration of fresh water — consistent with a typical condition in a natural stratified reservoir. The volumetric inflow rate is $Q = U_{\text{in}} h_{\text{in}} B_{\text{in}} = 0{,}09$ m$^3$/s, which, relative to the critical plunge discharge computed from the Knapp and Akiyama–Stefan [21] theory, $Q_{\text{cr}} = B_{\text{in}} \sqrt{g' h_{\text{in}}^3} \approx 0{,}141$ m$^3$/s, gives $Q/Q_{\text{cr}} \approx 0{,}64$, i.e. the flow is in the subcritical inflow regime. The Froude number of the incoming flow is

$$\text{Fr}_{\text{in}} = \frac{U_{\text{in}}}{\sqrt{g' h_{\text{in}}}} = \frac{0{,}5}{\sqrt{0{,}763 \cdot 0{,}3}} \approx 1.05,$$

indicating that the flow lies near the critical limit (Fr = 1). The inflow Reynolds number computed from the effective viscosity, $\text{Re}_{\text{in}} = U_{\text{in}} h_{\text{in}} / \nu_{\text{eff}} = 1500$, represents the fully turbulent regime of the real flow through a parameterized turbulent mixing.

During the computation the maximum Courant number was $C_{\max} = 0{,}40$, and the adaptive step remained below the bound $Co_{\max} = 0{,}5$ for almost the entire time; the 30 s simulation was carried out in $N = 1011$ steps with a mean step $\overline{\Delta t} \approx 0{,}030$ s. To ensure a reliable solution of the pressure Poisson equation in regions of sharp density gradients, the number of PCG iterations was increased to 60.

The evolution of the concentration field in the longitudinal cross-section reveals the classical stages of the plunging process (Figure 2). Around $t \approx 3.5$ s the plume leaves the inlet and first spreads in the horizontal direction; its density is appreciably higher than that of the upper layer but also exceeds that of the lower layer. In the interval $t \approx 7 \div 10$ s the plume turns downward under its own weight and the plunge point forms; at this point

the vertical velocity reaches $w \approx -0{,}08$ m/s, i.e. about 16% of the incoming horizontal velocity — in agreement with the laboratory estimate of Ellison–Turner [21]. By $t \approx 12$ s the plume reaches the interface level ($z \approx 0{,}7$ m), partially breaks it and descends into the lower layer; in the final state at $t = 30$ s the plume occupies about 70% of the domain length.

The velocity field fully reveals the hydrodynamic structure of the plunging process (Figure 3). Near the inlet ($x < 1$ m) the flow is almost horizontal, retaining $u \approx U_{\text{in}}$, and drives a strong return flow in the lower layer. Around the plunge point a convergent streamline pattern forms and the velocity vector deflects downward. Beyond the plunge point the flow attaches to the bed and develops as a dense bottom current (underflow); in this current the maximum velocity is about 0,3 m/s ($\approx 60\%\, U_{\text{in}}$), reflecting the partial conversion of inertial energy into gravitational potential energy.

The deviation of the pressure field from the hydrostatic level shows the hydrodynamic response to the plume inflow (Figure 4). Around the inlet the pressure rises by about +350 Pa (the gradient required for the incoming mass flow), while beneath the plunge point it drops to about −150 Pa (consistent with the Bernoulli balance of the strong vertical velocity). These spatial patterns agree with measured results (Hauenstein and Dracos [21]) and confirm that the projection step removes the divergence to the order of $\sim 10^{-5}$ at every step, i.e. the flow remains practically incompressible.

The averaged concentration at the outflow boundary $\alpha_{\text{out}}(t)$ shows the approach of the flow regime to a steady state (Figure 5). For $t < 1$ s, $\alpha_{\text{out}} \approx 0$; in the interval $1 < t < 5$ s the plume reaches the outlet and $\alpha_{\text{out}}$ rises rapidly, after which it slowly approaches the asymptotic value $2{,}64 \times 10^{-2}$. The final ratio is $\alpha_{\text{out}}/\alpha_{\text{in}} \approx 0{,}264$, i.e. the outflowing water carries away only about 26% of the inflow concentration; the remaining $\sim 74\%$ accumulates in the domain and forms an intrusion layer near the interface. This indicates that $t_{\text{end}} = 30$ s is limited for a fully steady state (a fully steady state requires about $60 \div 100$ s).

The integrated mass balance was found to satisfy the relation $\dfrac{dM}{dt} = Q_{\text{in}}\alpha_{\text{in}} - Q_{\text{out}}\overline{\alpha}_{\text{out}}$, with a relative balance error below $10^{-3}$. This level provides fully sufficient conservation for practical purposes in an open-boundary domain.

To assess the local stability, the vertical profile of the Richardson number,

$$Ri(z) = \frac{-\,g\,\partial\overline{\rho}/\partial z}{\rho_0\,(\partial\overline{u}/\partial z)^2},$$

was constructed from the density and velocity fields averaged over time and the horizontal directions (Figure 6). By the classical Miles–Howard criterion, linear stability is ensured in the regime $Ri > 0{,}25$. In the numerical result $Ri$ takes positive values throughout the depth; near the bed ($z < 0{,}15$ m) $Ri \approx 0{,}16 \div 0{,}23$ (slightly below the critical limit, associated with the shear of the dense bottom current), around the interface ($z \approx 0{,}3 \div 0{,}4$ m) $Ri \approx 20 \div 25$ (the strong preservation of the density jump), and in the upper layer $Ri \approx 1 \div 5$. Overall, $Ri > 0{,}25$ at about 90% of the nodes (the stable regime) and $0 < Ri < 0{,}25$ at about 10% (potentially unstable but not linearly unstable). This explains why no strong KH "mushroom" phenomenon is observed during the simulation: the stabilizing effect of phase separation and the parameterized turbulent diffusion prevent a complete breakdown of the stratification.

Finally, Figure 7 presents a combined overview of the final state, bringing together the concentration field, the velocity field, the outflow-concentration history and the Richardson-number profile in a single panel.

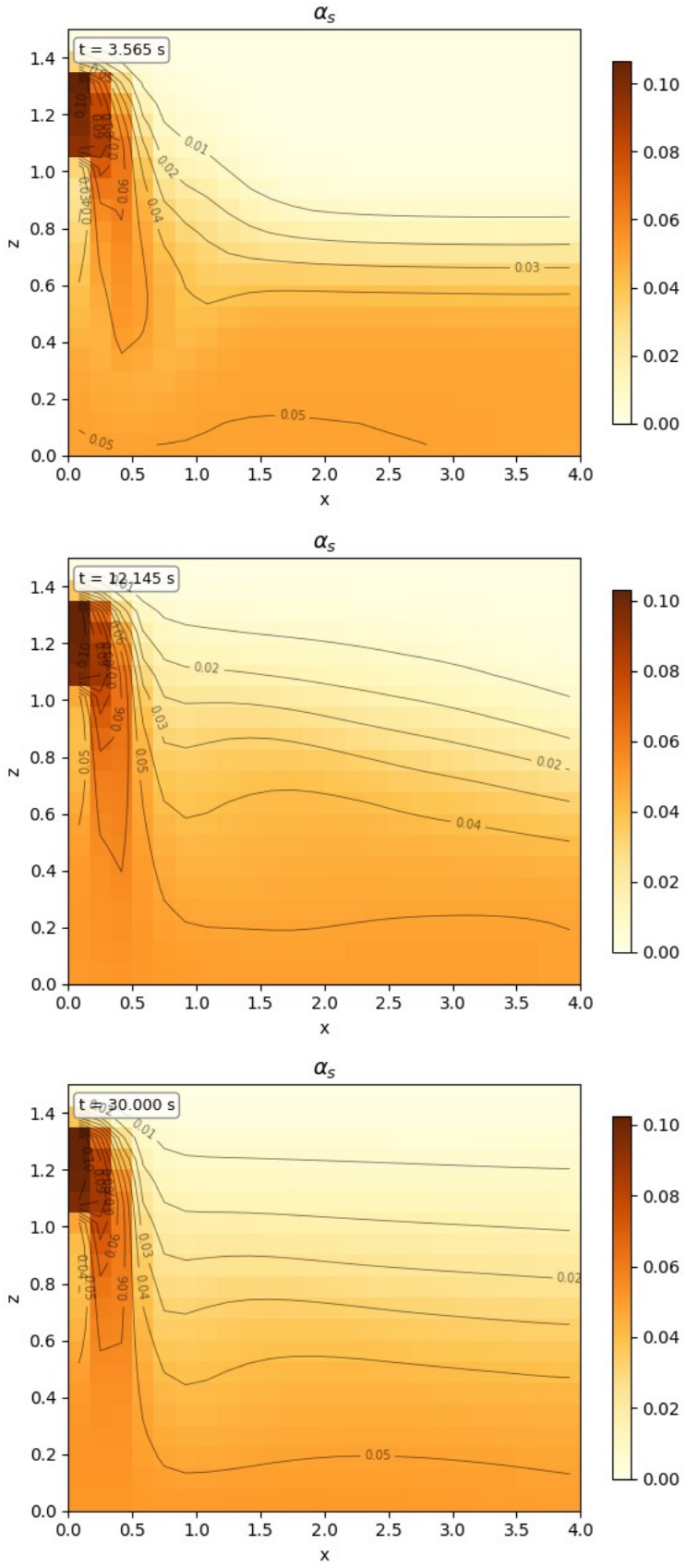


**Figure 2** Time evolution of the concentration field $\alpha_2$ in the longitudinal cross-section $y = L_y/2$ at five instants ($t = 0$; 3,565; 7,800; 12,145; 30,000 s): inflow, horizontal spreading, formation of the plunge point and approach to the steady regime

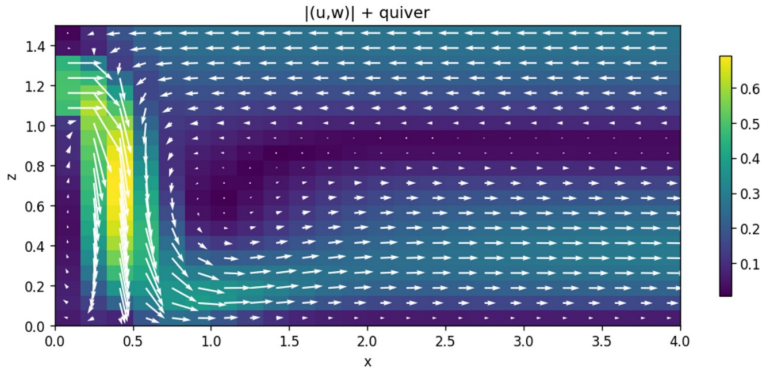


**Figure 3** Final distribution of the velocity field $|\mathbf{u}|$ with velocity vectors: inflow, plunge convergence and dense bottom current

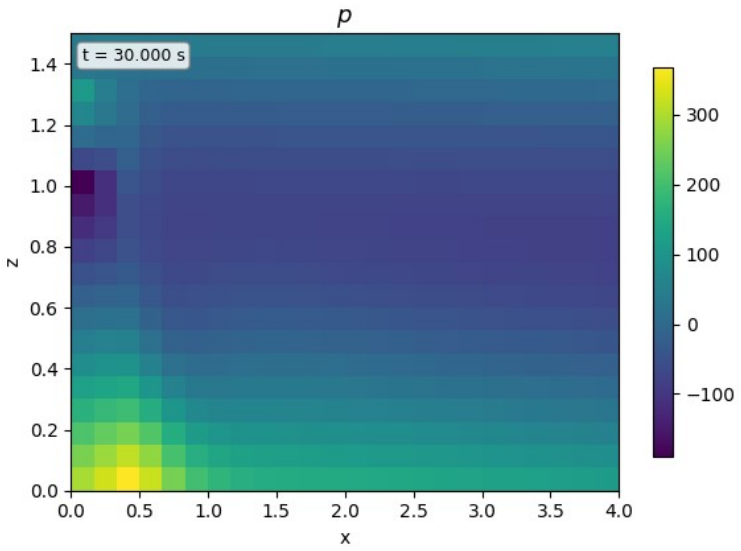


**Figure 4** Pressure perturbation: the high-pressure zone near the inlet and the low-pressure trough beneath the plunge point

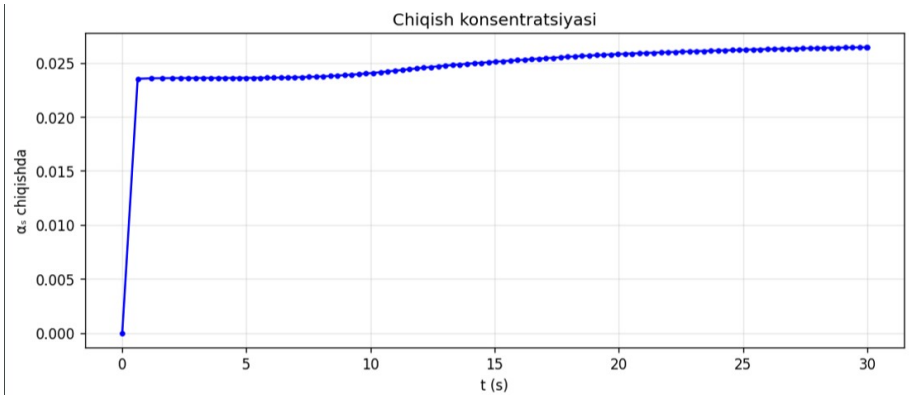


**Figure 5** Time variation of the averaged outflow concentration $\alpha_{\text{out}}(t)$

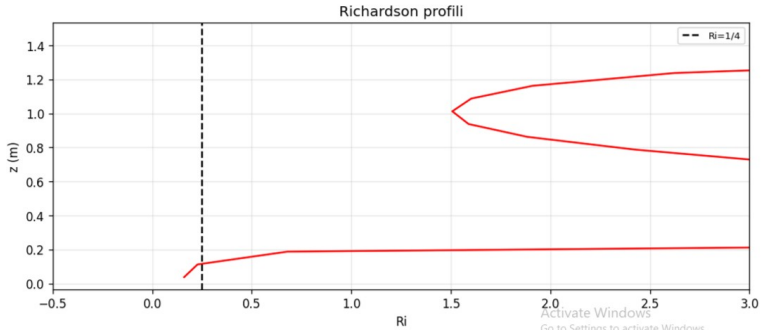


**Figure 6** Vertical profile of the Richardson number $Ri(z)$ (the Miles–Howard critical limit $Ri = = 0{,}25$ is shown as a dashed line): low values near the bed (flow shear) and strong maxima around the interface (density jump)

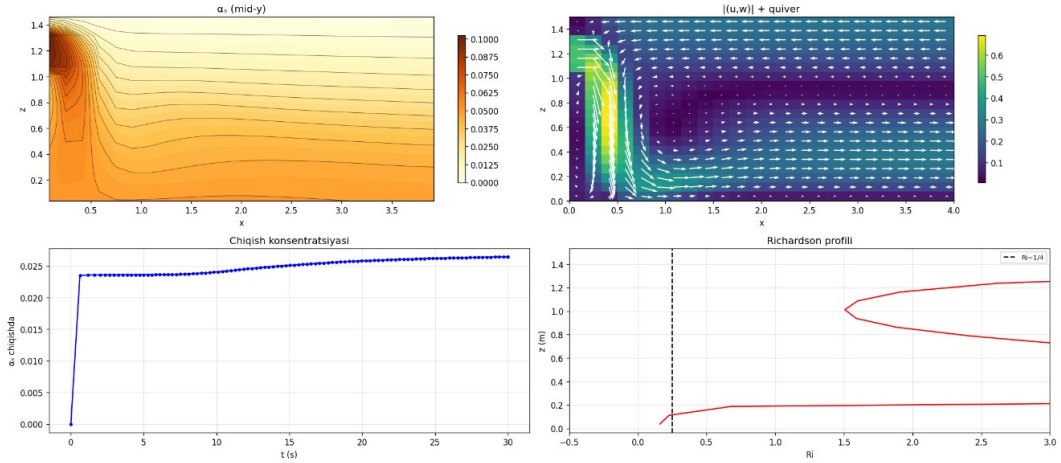


**Figure 7** Combined overview of the final state: concentration field, velocity field, outflow-concentration history and Richardson-number profile

**Table 3** Main variables and parameters of the model

| Quantity | Numerical result | Classical estimate / source |
|---|---|---|
| Critical plunge discharge $Q_{\text{cr}}$ | 0.141 $\text{m}^3/\text{s}$ | Akiyama–Stefan [21] |
| Regime $Q/Q_{\text{cr}}$ | 0.64 (subcritical) | $< 1$ — plunging [21] |
| Inflow Froude number $\text{Fr}_{\text{in}}$ | 1.05 | $\approx 1$ (critical limit) |
| Plunge velocity $\lvert w \rvert$ | 0.08 m/s (16% $U_{\text{in}}$) | 15–20% $U_{\text{in}}$, Ellison–Turner [22] |
| Max. underflow velocity | 0.30 m/s (60% $U_{\text{in}}$) | 50–70% $U_{\text{in}}$ [23] |
| Pressure rise / drop | $+350$ / $-150$ Pa | Hauenstein–Dracos [23] |
| Fraction of nodes with $\text{Ri} > 0.25$ | $\sim 90\%$ | Miles–Howard stability |
| Relative mass-balance error | $< 10^{-3}$ | — |

To assess the reliability of the results, the main integral quantities were compared with classical laboratory and theoretical estimates (Table 3). For all quantities the numerical results match the expected physical ranges, which confirms the physical correctness of the model and of the numerical scheme.

Thus, the results confirm that the balance between two competing mechanisms — phase separation (stabilizing, increasing $Ri$) and the velocity shear induced by the river flow (destabilizing, decreasing $Ri$) — determines the solution of the problem.

## 5 Conclusion

In this work the dynamics of the inflow of a multiphase (turbid) river flow into a stratified reservoir, phase separation, and the breakdown of the layered structure were posed mathematically in three-dimensional geometry on the basis of Kh.A. Rakhmatulin's full two-fluid model. Unlike the Boussinesq approximation, each of the two phases has its own velocity field, and the drag force between them directly represents phase separation; the vertical mixing was tied to the local Richardson number, and near the bed re-erosion was introduced through the Garcia–Parker formula.

The problem was solved on a Harlow–Welch staggered grid by a five-stage adaptive scheme based on operator splitting: TVD reconstruction for advection, Crank–Nicolson/ADI for diffusion, and a projection method (Poisson equation by the PCG method) for the pressure–velocity coupling. A simulation of the subcritical plunging regime in a laboratory-scale basin ($Fr_{\text{in}} \approx 1{,}05$, $Q/Q_{\text{cr}} \approx 0{,}64$) correctly separated three distinct stages — upper-layer spreading around the inlet, vertical deepening at the plunge point, and a dense current along the bed. The results were verified against classical plunging criteria (Knapp, Akiyama–Stefan), the plunge velocity (Ellison–Turner), the pressure patterns (Hauenstein–Dracos), the Miles–Howard stability condition, and the mass balance (relative error $< 10^{-3}$). The only notable limitation is that $t_{\text{end}} = 30$ s is too short to reach a fully steady state: $\alpha_{\text{out}}$ has not yet fully reached its asymptote. Future work should examine, through computations over $t_{\text{end}} \sim 100 \div 200$ s, the transition of the inflow plume to periodic oscillations or the formation of a stable intrusion layer, as well as the application of the developed architecture to the selective-withdrawal regime [20].

## References

[1] Bitsadze A.V., Salakhitdinov M.S. *On the theory of equations of mixed-composite type* // *Siberian Mathematical Journal.* – Novosibirsk, 1961. – Vol. 2. – № 1. – P. 7–19.

[2] Islomov B.I., Ochilova N.K., Sadarangani K.S. *On a Frankl-type boundary value problem for a mixed-type degenerating equation* // *Ukrainian Mathematical Journal.* – 2019. – P. 1347–1359.

[3] Islomov B.I., Usmonov B. *Nonlocal boundary value problem for a third-order equation of elliptic-hyperbolic type* // *Lobachevskii Journal of Mathematics.* – 2020. – № 41(1). – P. 32–38.

[4] Abdullaev O.K. *On a problem for the degenerating parabolic-hyperbolic equation involving Caputo derivative of fractional order and non-linear terms* // *Uzbek Mathematical Journal.* – 2021. – P. 5–16.

[5] Yuldashev T.K., Islomov B.I., Alikulov E.K. *Boundary value problems for a loaded parabolic-hyperbolic equation in infinite three-dimensional domains of third order* // *Lobachevskii Journal of Mathematics.* – 2020. – № 41(5). – P. 926–944.

[6] Ochilova N.K., Yuldashev T.K. *On a nonlocal boundary value problem for a degenerate parabolic-hyperbolic equation with fractional derivative* // *Lobachevskii Journal of Mathematics.* – 2022. – Vol. 1. – P. 229–236.

[7] Chanillo S., Wheeden R.L. *Existence and estimates of Green's function for degenerate elliptic equations* // *Annali della Scuola Normale Superiore di Pisa.* – 1988. – Vol. 15. – № 2. – P. 309–340.

[8] Vishik M.I., Grushin V.V. *On a class of higher order degenerate elliptic equations* // *Sbornik Mathematics*. – 1969. – Vol. 9. – № 4. – P. 423–454.

[9] Levendorskiĭ S.Z. *Degenerate elliptic equations and boundary problems* // *Springer Lecture Notes in Mathematics*. – 1992. – P. 25–47.

[10] Drábek P. *Solvability of degenerate elliptic problems of higher order via Leray–Schauder degree* // *Hiroshima Mathematical Journal*. – 1996. – Vol. 26. – Issue 1. – P. 1–14.

[11] Beisebay P., Berdyshev A., Omarov B. *Smoothness of the solution of a boundary value problem for degenerate elliptic equations* // *Symmetry*. – 2025. – Vol. 17. – № 9.

[12] Baishemirov Z., Berdyshev A., Ryskan A. *A solution of a boundary value problem with mixed conditions for a four-dimensional degenerate elliptic equation* // *Mathematics*. – 2022. – Vol. 10. – № 7. – Art. 1094.

[13] Zhang G. *The Kato problem and extensions for degenerate elliptic operators of higher order in weighted spaces* // *arXiv preprint arXiv:2511.04046*. – 2025.

[14] Irgashev B.Yu. *Boundary value problem for a degenerate high-order equation with discontinuous coefficients* // *Uzbek Mathematical Journal*. – 2021. – Vol. 65. – № 4. – P. 13–26.

[15] Pankov V.V., Baev A.D., Kharchenko V.D. *A priori estimate of solutions of one boundary-value problem in a strip for a higher-order degenerate elliptic equation* // *Journal of Mathematical Sciences*. – 2022.

[16] Ergashev T.G. *Potentials for singular elliptic equations and their applications* // *Russian Mathematics (Izvestiya VUZ. Matematika)*. – 2009. – № 53(8). – P. 46–57.

[17] Le V.K. *On boundary value problems for degenerate quasilinear elliptic equations of higher order* // *Nonlinear Analysis*. – 1998. – Vol. 31. – № 3. – P. 441–456.

[18] Pukal'skii I.D., Yashan B.O. *Optimal control in the boundary value problem for elliptic equations with degeneration* // *Mathematical Studies*. – 2023. – Vol. 60. – № 2. – P. 45–58.

[19] Barton A. *Boundary-value problems for higher-order elliptic equations* // *Higher-Order Elliptic Equations and Systems. Springer*. – 2013. – P. 99–122.

[20] Mukhamedov A., Yusupov F.A. *Analysis of some boundary value problems for mixed-type equations with two lines of degeneracy* // *Irish Interdisciplinary Journal of Science and Research*. – 2022. – Vol. 6. – № 2. – P. 87–96.

[21] Witt I. *A calculus for a class of finitely degenerate pseudodifferential operators* // *Banach Center Publications*. – 2003. – Vol. 60. – P. 295–317.

[22] Ellison T.H., Turner J.S. *Turbulent entrainment in stratified flows* // *Journal of Fluid Mechanics*. – 1959. – Vol. 6. – № 3. – P. 423–448.

УДК 519.6

# МАТЕМАТИЧЕСКОЕ МОДЕЛИРОВАНИЕ ПОСТУПЛЕНИЯ МНОГОФАЗНОГО ПОТОКА СМЕСИ В СТРАТИФИЦИРОВАННОЕ ВОДОХРАНИЛИЩЕ И РАЗРУШЕНИЯ СЛОИСТОЙ СТРУКТУРЫ

[1] ***Яхшибаев Д.С.,*** [2*] ***Боборахимов Б.И.***

[*]uzbekpy@gmail.com

[1]Ташкентский университет информационных технологий имени Мухаммада-ал-Хоразмий, 100202, Узбекистан, Ташкент, ул. Амира Темура, 108.

[2]Научно-исследовательский институт развития цифровых технологий и искусственного интеллекта,
100125, Узбекистан, г. Ташкент, Мирзо-Улугбекский р-он, м-в Буз-2, д. 17А.

Предложена трёхмерная математическая модель поступления мутного (несущего наносы) речного потока в плотностно-стратифицированное водохранилище с учётом разделения фаз и разрушения слоистой структуры. Модель основана на теории взаимопроникающих континуумов Х.А. Рахматулина: несущая жидкость и дисперсные частицы обладают каждая своим полем скоростей, а сила межфазного взаимодействия описывает осаждение частиц. Коэффициент вертикального перемешивания задаётся как функция локального числа Ричардсона, что учитывает разрушение стратификации вследствие неустойчивости Кельвина–Гельмгольца; переразмыв осевших частиц у дна моделируется по формуле Гарсиа–Паркера. Задача решается на смещённой сетке Харлоу–Уэлча пятиэтапной схемой расщепления по операторам. Моделирование субкритического режима ныряния воспроизводит входную струю, точку ныряния, придонное течение и интрузионный слой; результаты подтверждены классическими критериями и балансом массы.

**Ключевые слова:** стратифицированное водохранилище, многофазный поток, модель Рахматулина, разделение фаз, мутьевой поток, ныряние, число Ричардсона, неустойчивость Кельвина–Гельмгольца, расщепление по операторам, переразмыв, формула Гарсиа–Паркера.

**Цитирование:** *Яхшибаев Д.С., Боборахимов Б.И.* Математическое моделирование поступления многофазного потока смеси в стратифицированное водохранилище и разрушения слоистой структуры // Проблемы вычислительной и прикладной математики. – 2026. – № 3(73). – С. 7-24.

**DOI:** https://doi.org/10.71310/pcam.3_73.2026.01

№ 3(73) 2026

ISSN 2181-8460

# HISOBLASH VA AMALIY MATEMATIKA MUAMMOLARI

## ПРОБЛЕМЫ ВЫЧИСЛИТЕЛЬНОЙ И ПРИКЛАДНОЙ МАТЕМАТИКИ

## PROBLEMS OF COMPUTATIONAL AND APPLIED MATHEMATICS

AiRI
RAQAMLI TEXNOLOGIYALAR VA SUN'IY INTELLEKTNI RIVOJLANTIRISH ILMIY-TADQIQOT INSTITUTI

# ПРОБЛЕМЫ ВЫЧИСЛИТЕЛЬНОЙ И ПРИКЛАДНОЙ МАТЕМАТИКИ

## № 3(73) 2026

Журнал основан в 2015 году.
Издается 6 раз в год.

**Учредитель:**
Научно-исследовательский институт развития цифровых технологий и искусственного интеллекта.



Журнал зарегистрирован в Агентстве информации и массовых коммуникаций при Администрации Президента Республики Узбекистан.
Свидетельство №0856 от 5 августа 2015 года.

**ISSN 2181-8460, eISSN 2181-046X**



**Адрес редакции:**
100125, г. Ташкент, м-в. Буз-2, 17А.
Тел.: +(998) 71 263-41-98.
Э-почта: journals@airi.uz.
Веб-сайт: https://journals.airi.uz.

**Дизайн и вёрстка:**
Шарипов Х.Д.

Отпечатано в типографии НИИ РЦТИИ.
Подписано в печать 25.06.2026 г.
Формат 60x84 1/8. Заказ №3. Тираж 100 экз.

# PROBLEMS OF COMPUTATIONAL AND APPLIED MATHEMATICS

## No. 3(73) 2026

The journal was established in 2015.
6 issues are published per year.

**Founder:**
Digital Technologies and Artificial Intelligence Development Research Institute.



The journal is registered by Agency of Information and Mass Communications under the Administration of the President of the Republic of Uzbekistan.
Certificate of Registration No. 0856 of 5 August 2015.

**ISSN 2181-8460, eISSN 2181-046X**



**Address:**
100125, Tashkent, Buz-2, 17A.
Tel.: +(998) 71 263-41-98.
E-mail: journals@airi.uz.
Web-site: https://journals.airi.uz.

**Layout design:**
Sharipov Kh.D.

DTAIRI printing office.
Signed for print 25.06.2026
Format 60x84 1/8. Order No. 3. Print run of 100 copies.

# Содержание

# Contents